Nuclear Engineering and Design 120 (1990) 193–201
North-Holland

GAS ENTRAINMENT INCEPTION AT THE BORDER OF A FLOW-SWOLLEN LIQUID SURFACE

Haruki MADARAME and Tamotsu CHIBA

Department of Nuclear Engineering, The University of Tokyo, Bunkyo-ku, Tokyo 113, Japan

A rapid liquid flow into a tank may impinge on the free surface, making it swell partially. The returning flow branches off from the free surface and re-submerges at the border of the swollen surface. If the flow velocity along the swollen surface is high enough, gas bubbles are formed at the border and entrained by the liquid flow. The conditions necessary for gas entrainment in a simple system are examined experimentally, using water and air as working fluids. The effect of surface tension is examined by adding a surface active agent to the water. The results show that gas entrainment inception is determined by the flow pattern in the system and the product of the Froude and Weber numbers based on the local velocity at the bubble formation point.

1. Introduction

A number of flow problems arise when designing an economical, compact sodium-cooled fast breeder reactor with a high thermal output and associated high coolant flow rate. One of these is cover gas entrainment at the free surface of the sodium. If a significant concentration of gas is entrained by the sodium flow, bursts of gas bubbles may pass through the reactor core, causing a change in reactivity. The bubbles may inhibit the removal of heat from the fuel rods. Gas entrainment must be carefully prevented in fast breeder reactor design, although it is not possible to predict theoretically when it will occur.

The following three types of entrainment, illustrated in fig. 1, are considered possible in sodium-cooled reactors [1]:
(1) vortex formation,
(2) breaking of surface waves, and
(3) waterfall formation.
Gas entrainment at vortices in a liquid surface has been studied by many researchers [2–5], but there are few works that deal with gas entrainment in fast breeder reactors caused by the breaking of waves and by a waterfall. In this paper we describe an experimental study of gas entrainment caused by a small waterfall in a fast breeder reactor.

Fig. 2 is a schematic view of an intermediate heat exchanger (IHX) of a pool-type reactor. The primary coolant flows into the upper plenum through the openings in the shell and is distributed to the heat exchanger tubes. The plenum has a free surface where the coolant is in contact with the cover gas. Though the openings in the shell are submerged, the free surface is disturbed when the coolant velocity is high. The flow impinges on the central structure, which provides the secondary coolant flow paths, and some of the coolant flows along

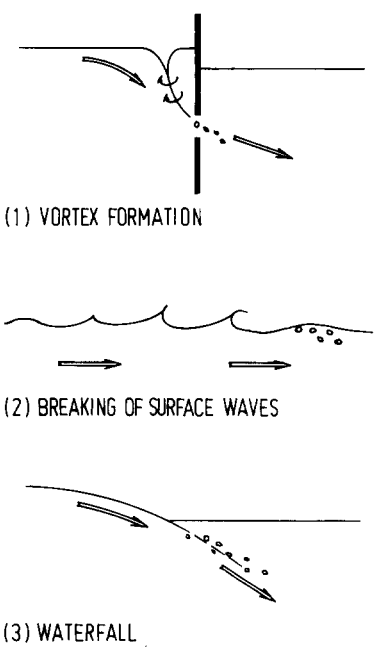

Fig. 1. Possible types of cover gas entrainment in fast breeder reactors.

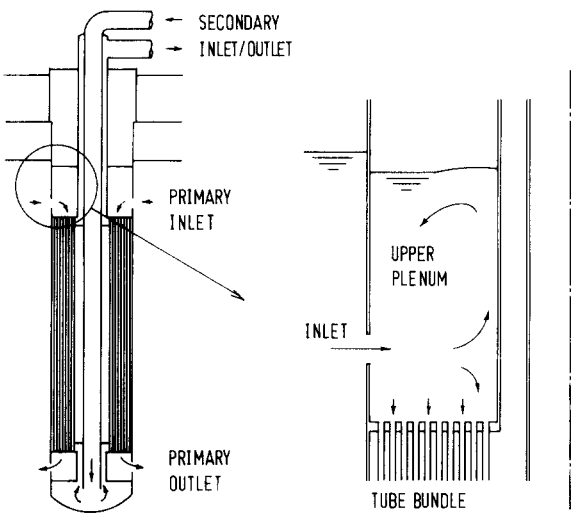

Fig. 2. Schematic view of IHX in a pool-type reactor.

the structure toward the free surface, making it swell partially. The coolant then flows down the swollen surface like a small waterfall and returns to the shell. Since the slope of the surface is discontinuous at the border of the swollen part, the flow branches away from the surface and re-submerges there. The slope discontinuity leads to the formation of gas bubbles, which are entrained by the re-submerging flow. The flow along the swollen surface can be regarded as a small waterfall; thus, the phenomenon is considered to be a waterfall-induced entrainment.

The gas entrainment problem caused by the entry of a falling film into a pool has been studied theoretically in the case of laminar flow [6]; however, the recirculating flow in the IHX upper plenum is turbulent. Measurements have been made of the quantity of gas entrained by a turbulent jet plunging through the gas and entering a pool of stationary water [7], but no importance has been attached to clarifying gas entrainment inception. The entering jet decelerates rapidly in the pool, whereas the recirculating flow in the plenum does very little after re-submergence. Though the mechanisms of bubble formation are the same in both cases, there is a difference in the entrainment behavior following the formation. Sodium is used as a coolant in fast breeder reactors, while most entrainment experiments have used water as a working fluid. An experimental study is needed using a model geometrically similar to the plenum that aids our understanding of the correlation between fluids of different physical properties.

A waterfall will appear not only in this particular plenum but in any plenum when there is a strong circulation that causes the free surface to swell partially. Waterfall-induced entrainment can be avoided by a reduction in velocity, which requires a larger, more expensive plenum. The purpose of the present study is to show quantitatively gas entrainment inception caused by a waterfall.

2. Experimental method

The coolant flow in the diametrical section of the IHX upper plenum was simulated in a thin, rectangular test section (fig. 3). In the plenum, there is radial and circumferential flow of coolant; however, of these two flows, only the radial flow could be simulated in the test section, this being represented by the flow of the simulated coolant parallel with the transparent walls of the test section. Also, in practice, a local secondary flow occurred at each corner of the test section. However, despite these differences, waterfall-induced entrainment was well simulated in the test section (see fig. 3). The flow in the parallel transparent-walls was substituted for the radial flow in the plenum. The coolant can flow circumferentially in the plenum, whereas it could flow only in the plane parallel to the transparent walls in the test section. The transparent walls caused a local secondary flow at the corner. However, the waterfall-induced entrainment was well simulated in the test section.

The simulated coolant flowed in through a rectangular inlet hole on one side of the test section and out through many 10 mm diameter holes uniformly bored in the bottom plate. The vertical distance between the center of the inlet and the bottom plate was 400 mm.

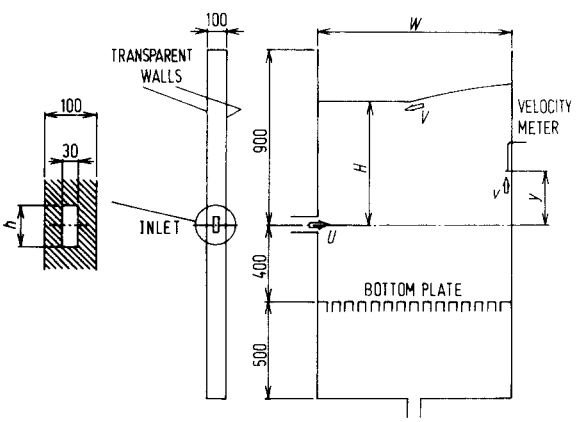

Fig. 3. Test section.

Table 1
Experimental conditions

	Fluid	H [mm]	W [mm]	h [mm]	D_e [mm]
Case 1	water	100 ~ 800	1000	80	43.6
Case 2	water	100 ~ 800	750	80	43.6
Case 3	water	100 ~ 800	500	80	43.6
Case 4	water	100 ~ 800	750	50	37.5
Case 5	water	100 ~ 800	750	30	30.0
Case 6	water with sodium oleate	100 ~ 800	750	80	43.6

The inlet width of 30 mm was smaller than the test section thickness of 100 mm; therefore the flow was not two-dimensional near the inlet. The bottom plate holes led to 50 mm long pipes; thus, the flow in the space below the plate did not affect the flow pattern in the test section. The height of the non-swollen free surface from the inlet center, H, the width of the test section, W, and the height of the inlet hole, h, were parametrically varied to investigate the effect of scale (table 1). Case 2 is the standard; the effect of the test section width is examined in Cases 1 and 3. Cases 4 and 5 are planned to investigate the effect of the inlet height. The number of bottom holes was 115 when the test section width was 1000 mm.

Water was used as the simulated coolant in the experiment. The relevant modeling groups are generally the Froude, Weber, and Reynolds numbers, which correlate among fluids of different physical properties. The entrainment inception at a turbulent vortex has been shown by Baum and Cook [3] to be primarily a function of the Froude and Weber numbers, with no dependence on the Reynolds number. In other words, viscosity does not affect the onset conditions of turbulent gas entrainment at a vortex. Though the global flow pattern in the case of vortex-induced entrainment is different from that in the case of waterfall-induced entrainment, the similarity in the local flow behavior leading to bubble formation indicates that the viscosity difference has no effect on waterfall-induced entrainment. In both cases the gas tip would occasionally break away because of the high velocity gradient, forming a few bubbles. Since the viscous stresses are negligible compared with the turbulence stresses in turbulent flows, viscosity difference does not affect the coolant motion as long as the flow is turbulent. Considering the above fact, no experiment was planned to investigate the effect of viscosity difference.

The effect of surface tension was examined by adding a surface active agent, 0.1% sodium oleate, to the water. Fig. 4 shows the variation of the surface tension of water with sodium oleate concentration [8]. It varies little from 0.035 N/m, when the concentration is around 0.1%. It changes with time soon after the dissolution of the sodium oleate, but becomes stable after 100 min. The viscosity is not affected while the concentration is below 10%. Comparing the result with that for water having a surface tension of 0.074 N/m at 10°C, an expression for the entrainment inception condition can be determined as a function of the Froude and Weber numbers. The Case 6 experiment (table 1) makes use of the surface active agent.

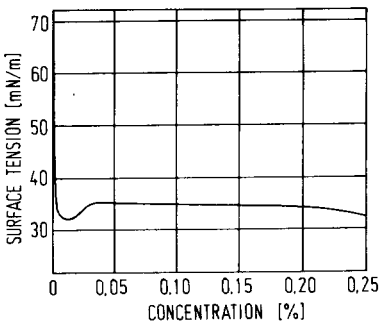

Fig. 4. Variation of surface tension of water with sodium oleate concentration.

The loop shown in fig. 5 could supply about 1000 l/min of water to the test section. In order to keep the water level in the test section constant, the inlet and outlet flow rates were controlled carefully by upstream and downstream valves, respectively. The gas entrainment could be observed with the naked eye through the transparent walls of the test section. The entrainment

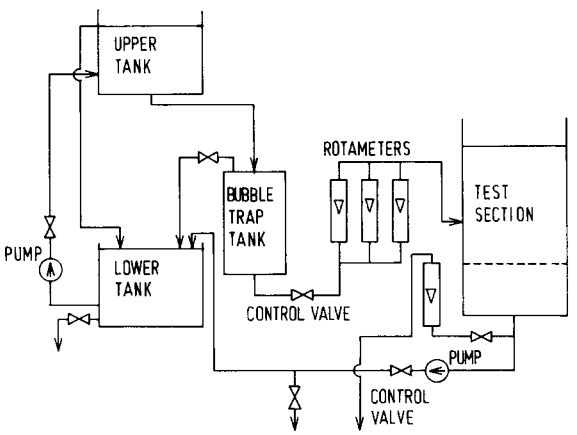

Fig. 5. Experimental water loop.

occurred at random because of turbulence, which made recognition of the entrainment inception difficult. Entrainment was deemed to have occurred when it had been observed more than once every 10 s during the experiment, constant conditions having been maintained for 5 min.

The flow pattern in the test section was observed in order to obtain information about the local flow behavior near the bubble formation point, using polystyrene tracer particles. It was planned to measure the fluid velocity near the bubble formation point, but the turbulent behavior made it very difficult. Therefore the upward velocity at various positions 3 cm from the impingement wall of the test section was measured with miniature propeller flow meters (windmill-type velocity meters having a propeller outer diameter of 3 mm, a measuring range of 2.5–100 cm/s, and an accuracy of 1%) in order to estimate the bubble formation point flow velocity. Data were obtained for Cases 2, 3, 4, and 5 with various flow rates and free surface levels. The velocity fluctuated because of turbulence; therefore the average value of about 20 measurements taken at intervals of 1 s was calculated under each condition.

3. Experimental result

3.1. Flow pattern

The flow patterns in the test section could be grouped into the following three types (fig. 6) based on the flow near the free surface:

(1) countercurrent with very small or no waterfall (Pattern A),
(2) countercurrent with waterfall (Pattern B), and
(3) direct flow from the inlet (Pattern C).

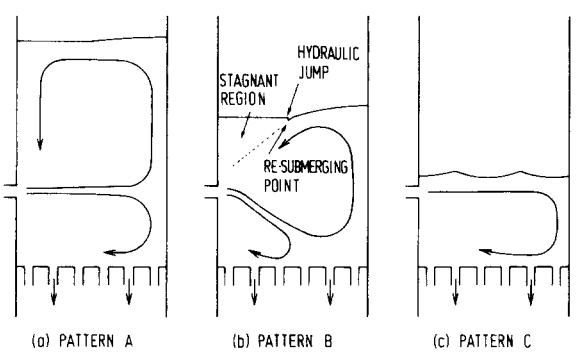

Fig. 6. Flow patterns in test section.

Pattern A appeared when the inlet was deep in the water. The horizontal jet from the inlet impinged on the opposite wall directly. A major part of the fluid flowed upward along the impingement wall, then back to the inlet wall along the free surface. Another part flowed downward from the impingement point on the wall; thus, upper and lower swirls existed in opposite directions.

Pattern B appeared when the water was shallower. The inlet jet deflected downward before impingement on the wall; thus, the lower swirl was reduced in size. The upward flow from the impingement point made the free surface swell partially, and the returning flow branched off from the surface at the border of the swollen part. There was stagnant or slowly moving fluid in the area enclosed by the re-submerging flow, the non-swollen surface, and the inlet wall. The surface situation was quite similar to that in the case of transition from a shooting flow to an ordinary flow. The surface was depressed at the re-submerging point because of a high dynamic head and an associated low static head, and a hydraulic jump appeared between the re-submerging flow and the stagnant fluid. The surface of the jump was usually covered by bubbles, even in the case where there was no entrainment.

When the inlet was located near the free surface, Pattern C appeared. The fluid flowed from the inlet to the impingement wall along the free surface, with the breaking of waves.

It was difficult to draw a definite boundary between Patterns A and B. In the strict sense, the free surface of Pattern A was not flat but partially swollen, and a major portion of the returning flow branched off from the surface. Thus the grouping was not based on the flow condition near the surface but on the direction of the inlet jet impinging on the wall. On the other hand, the boundary between Patterns B and C was fairly clear. Fig. 7 is the flow pattern diagram for Case 1. Comparing these results with those in Cases 2 and 3, the aspect ratio, H/W, was found to be a factor determining the flow pattern. The pattern was little affected by the flow rate, Q; consequently, the results in every case could be similarly illustrated, regardless of the choice of abscissa between Q and the average inlet velocity, U.

Waterfall-induced entrainment occurred mainly in the case of Pattern B. The returning flow branched off from the surface midway between the inlet wall and the impingement wall, where bubbles were formed. Only when the flow rate was very high did a similar entrainment occur in the case of Pattern A. In the case of Pattern C, the gas was entrained by the breaking of waves. Though entrainment by the breaking of waves is

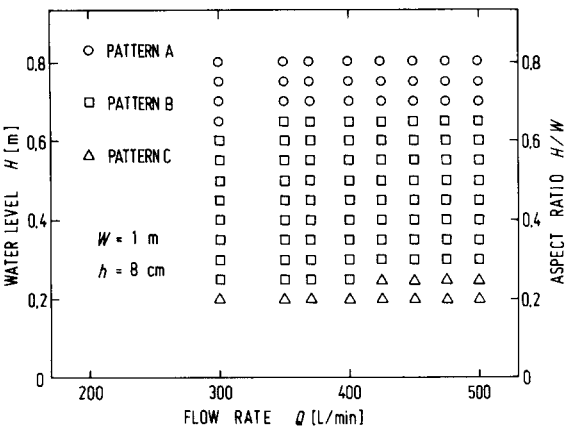

Fig. 7. Flow pattern diagram.

beyond the scope of this study, the entrainment inception in the case of Pattern C was examined as well as that in the cases of Patterns A and B.

The re-submerging flow carried the bubbles and joined the high-speed jet near the inlet. When the bubbles met the jet, they were fragmented by the strong inertial force. They were so small that they moved in the same manner as the liquid. Some recirculated in the upper swirl, while some drifted into the lower swirl and gradually flowed out through the bottom plate. Even if entrainment occurred only occasionally, the fragmented bubbles stayed in the test section for several minutes.

Vortex-induced entrainment was sometimes observed near the corners of the test section because of the local secondary flow mentioned earlier. Gas was occasionally entrained from thin layers of gas along the walls [4] of the test section because of the poor wetability of water. These types of entrainment could be distinguished easily from waterfall or breaking-wave-induced entrainment, and were not included in the data.

The local velocity at the re-submerging point is considered to be the most important condition necessary for gas entrainment. The velocity along the axis of a submerged round jet in infinite space, u_0, can be expressed as follows [9]:

$$u_0/U = 6.4D/x, \qquad (1)$$

where U is the initial velocity, x is the distance from the nozzle, and D is the diameter of the nozzle. In the test section, the jet from the inlet was bent by the impingement wall and was bent again by the free surface. The jet expansion in the direction perpendicular to the walls of the test section was restricted by the walls. If the expansion is fully two-dimensional, the axial velocity of the submerged jet is not inversely proportional to x but to the square root of x. Therefore, the above expression cannot readily be applied to the present phenomenon, but it is very instructive. Fig. 8 shows the upward velocity, v, on the impingement wall in Cases 2, 3, 4, and 5 for various flow rates and free surface levels. In the figure, the sum of the test section width and the vertical distance between the inlet and the measuring point, $W+y$, was defined as the distance from the inlet along the jet in order to compare the data with the values given by eq. (1). The jet did not impinge on the wall directly but deflected downward when Pattern B appeared. However, this effect was neglected in the arrangement of data. Since the jet was not round, the hydraulic diameter, D_e, was substituted for the diameter, D. Although the amount of scatter in measured values is large, eq. (1) for the flow path length $W+y$ and the hydraulic diameter, D_e, correlates well with the velocity near the impingement wall. Use of other equations and sizes does not give better correlation. It should be possible to estimate the velocity at the re-submerging point in a similar way. This was supported by the photographs of the tracer movement near the re-submerging point. Though the re-submerging velocity was obtained from the photographs, it was not correlated with the entrainment inception because of a large amount of scatter. The cause of the scatter was mainly the oscillation of the free surface and the steep velocity gradient at the re-submerging point.

3.2. Entrainment inception

The waterfall-induced gas entrainment region in Case 1 is shown in fig. 9 as an example. There was a lower flow-rate limit for the entrainment. In every case, an

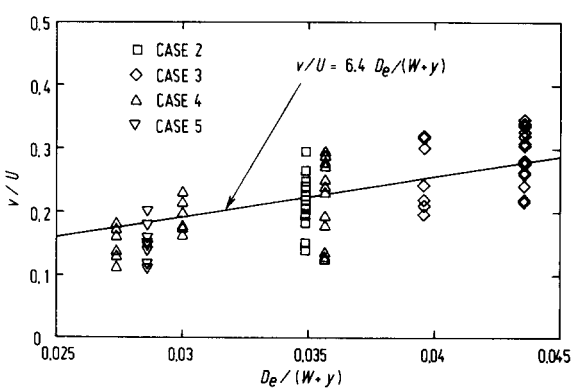

Fig. 8. Upward velocity on the impingement wall.

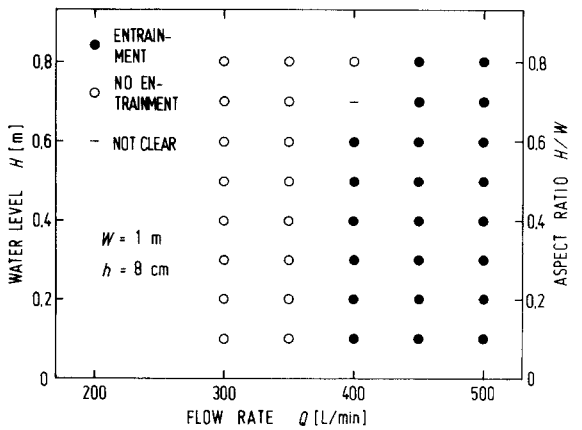

Fig. 9. Entrainment inception in Case 1.

increase in the water depth increased the flow rate for entrainment inception.

The velocity at the re-submerging point was considered to be a determining factor in entrainment. It could be estimated from the inlet velocity and the distance from the inlet along the streamline. Since the flow re-submerged mid-way between the inlet wall and the impingement wall, the distance along the streamline was represented by $W + H + 0.5W = 1.5W + H$. Using eq. (1), the re-submerging velocity, V, was estimated as follows:

$$V = 6.4U\frac{D_e}{1.5W + H}, \tag{2}$$

where U is the average inlet velocity and D_e is the hydraulic diameter of the inlet. Fig. 10 summarizes the entrainment inception when water without the surface active agent was used as a working fluid, only the data for which there was clear recognition of entrainment being plotted. The velocity necessary for the entrainment is a function of the aspect ratio, H/W, which governs the other determining factor, the re-submerging angle to the non-swollen surface.

A similar result was obtained in Case 6, using the surface active agent. The limit curve was biased toward lower velocity, though the dependency on the aspect ratio was almost the same. In order to express the entrainment inception conditions in a dimensionless form, the product of the local Froude number, $\mathrm{Fr} = V^2/gL$, and the local Weber number, $\mathrm{We} = \rho V^2 L/\sigma$, was defined as follows:

$$\mathrm{Fr} \cdot \mathrm{We} = \rho V^4/\sigma g, \tag{3}$$

where V is the re-submerging velocity estimated by eq. (2), ρ is the liquid density, σ is the surface tension, and g is the acceleration due to gravity. It should be noted

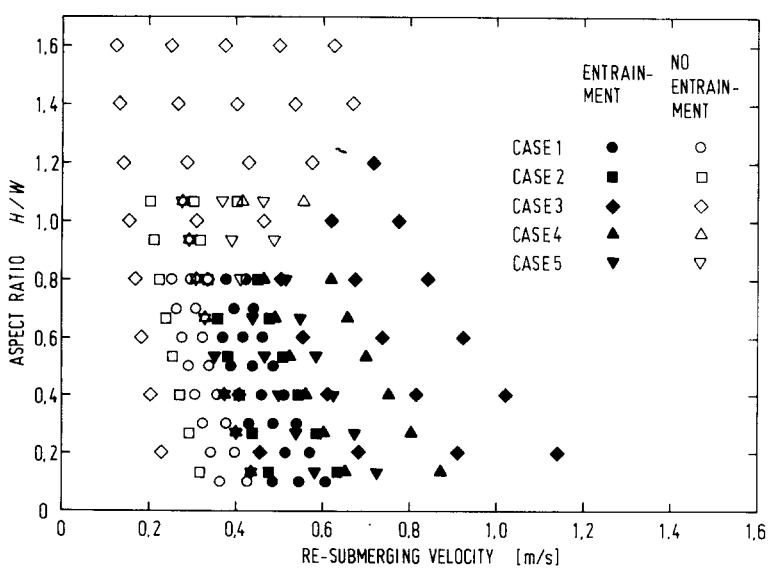

Fig. 10. Entrainment inception in various dimensions.

that the product does not involve any characteristic system dimension, L. The fourth root of the product was used as the abscissa in fig. 11, which expressed the entrainment inception by a single curve.

4. Discussion

Besides inertia, the forces that could be involved in the entrainment mechanism are gravitational, viscous, and surface tension forces. However, the molecular viscosity is considered to be negligible compared with the turbulence viscosity. The latter does not depend on the former but on the flow condition, which is represented by the velocity. Since the entrainment is dominated merely by the local flow conditions, no system dimensions are considered to affect the inception directly. The aspect ratio, H/W, only affects the re-submerging angle, θ, and consequently affects the entrainment. Thus, it may be assumed that the entrainment inception is a function of the re-submerging velocity, V; liquid density, ρ; surface tension, σ; and acceleration due to gravity, g, for a given re-submerging angle, θ. Buckingham's π theorem gives an expression for the condition for entrainment inception of the form:

$$\rho V^4/\sigma g = f(\theta). \tag{4}$$

The left side of the equation is the product of the Froude and Weber numbers.

The only characteristic dimension of the entrainment inception is the bubble diameter, which can be represented by $\sigma/\rho V^2$, since the bubbles are formed by the waterfall-induced shear force. Substituting this dimension in the Froude number, the same expression as the product of the Froude and Weber numbers is obtained. Therefore, the product can be interpreted as the Froude number according to the bubble diameter.

The velocity for the entrainment inception increases when the aspect ratio, H/W, is larger than 0.5. The flow pattern is affected by the ratio, and the re-submerging flow seems to have a small angle when the ratio is larger than 0.5. However, further discussion on the relation between the entrainment inception and the re-submerging angle cannot be made here, since the angle was not measured in this study.

There was a small difference of factor 2 in the surface tension of the working fluids in the experiment. It cannot be concluded from the experimental data that the entrainment inception velocity is proportional to the fourth root of the surface tension. The data only suggest that it is proportional to a value between the 0.2th power and the 0.3th power. But the data support the result of the dimensional analysis. For the extrapolation of the present result to the sodium flow, the difference of factor 2 is large enough, since the ratio of the surface tension of sodium to that of water is also around 2. The density of sodium is roughly the same as that of water. The viscosity of sodium is about a quarter that of water;

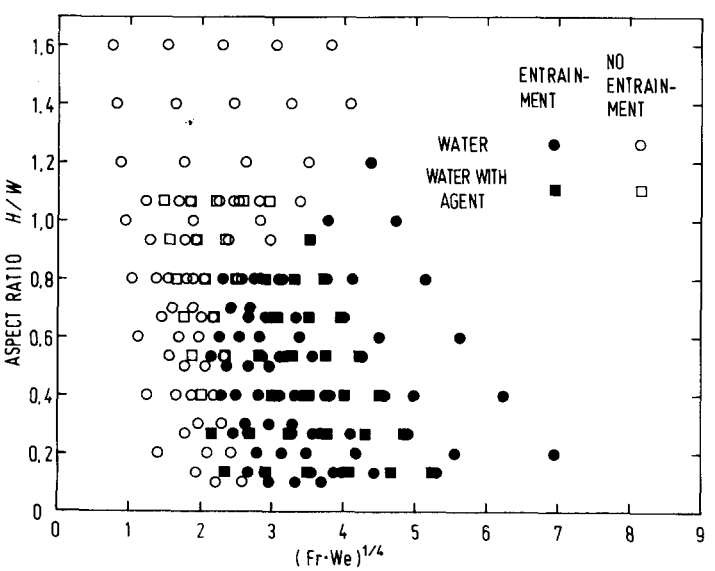

Fig. 11. Entrainment inception with different surface tensions.

consequently, the contribution of viscous force to the entrainment is considered to be smaller in the case of sodium. Therefore, the present result (fig. 11) seems to be applicable to entrainment in fast breeder reactors. However, the effect of viscosity on entrainment inception should be examined experimentally. It cannot be denied that viscosity affects the entrainment inception in some way.

In the present study, the re-submerging flow velocity was not measured directly but was estimated from the inlet velocity and the flow path length. With the use of the estimated re-submerging velocity, the gas entrainment inception is expressed by a single curve. This fact may suggest that the real re-submerging velocity is proportional to the estimated one. However, eq. (2) is considered to be applicable only for the present experimental conditions, especially for the present test section thickness and inlet width. The conditions for the entrainment inception should be correlated with the measured velocity and angle at the re-submerging point in order to widen the applicability of the result. Since measurement of the re-submerging velocity is difficult, some consideration is needed.

From the viewpoint of reactor design, tools for estimating the velocity profile in plenums with free surfaces are also needed. The turbulent flow problems for free surfaces are not readily solved by existing computer programs. If the programs are developed, the entrainment inception can be correlated with the re-submerging velocity and angle without direct measurement.

In a circular plenum, a circumferential flow which might affect the gas entrainment inception could appear. Experiments with a circular cross-section are also needed.

These are the subjects for future study.

5. Conclusion

When liquid flows into a tank at high velocity, the flow may impinge on the free surface directly or after deflection on the tank wall, causing the liquid surface to swell partially. The impinging liquid flows down the swollen surface like a waterfall and branches off from the surface at the border of the swollen part. If the re-submerging velocity is high, gas bubbles are formed and entrained by the re-submerging flow. Sodium-cooled fast breeder reactors have regions where a cover gas is in contact with the sodium. The gas entrained in the sodium flow may lead to operating problems in the reactors.

Experiments were performed to determine the conditions necessary for waterfall-induced entrainment inception using a thin, rectangular tank with an inlet on one side and an outlet at the bottom. Water was used to simulate the coolant, and the effect of surface tension was examined by adding a surface active agent, while that of viscosity was not examined experimentally since it was considered to be negligible. The inlet jet deflected on the impingement wall caused the surface to swell and the waterfall to form when the ratio of the water depth to the tank width was in a certain range. The entrainment conditions could be expressed by the aspect ratio and the product of the Froude and Weber numbers based on the re-submerging velocity.

The configuration of a real IHX upper plenum may be more complicated, and a different flow pattern may appear. Even in such cases, the gas entrainment can be predicted using the above information if the flow pattern can be calculated by numerical methods. The development of programs is another subject for future study.

Acknowledgment

The authors would like to acknowledge Mr N. Ogawa and Mr Y. Ueda for their assistance in the execution of the experiment.

Nomenclature

D = nozzle diameter,
D_e = hydraulic diameter of inlet hole,
Fr = Froude number, V^2/gL,
g = acceleration due to gravity,
H = free surface height from the inlet center,
h = height of inlet hole,
L = characteristic system dimension,
Q = flow rate,
U = average inlet velocity,
u_0 = jet velocity on the axis,
V = re-submerging velocity,
v = upward velocity near the impingement wall,
W = test section width,
We = Weber number, $\rho V^2 L/\sigma$,
x = distance from the nozzle,
y = height of measuring point from the inlet center,
θ = re-submerging angle,
ρ = liquid density,
σ = surface tension.

References

[1] J.M. Laithwaite and A.F. Taylor, Proc. IAEA Symp. on Sodium Cooled Fast Reactor Engineering, Monaco (1970) pp. 75–85.
[2] M.R. Baum, BNES J. 13 (2) (1974) 203–209.
[3] M.R. Baum and M.E. Cook, Nucl. Engrg. Des. 32 (1975) 239–245.
[4] M. Takahashi et al., J. Nucl. Sci. Technol. 25 (2) (1988) 131–142.
[5] M. Takahashi et al., J. Nucl. Sci. Technol. 25 (3) (1988) 245–253.
[6] D.R. Wilson and A.F. Jones, J. Fluid Mech. 128 (1983) 219–230.
[7] D.A. Ervine and E.M. Elsawy, Symposium on Design and Operation of Siphons and Siphon Spillways, London (1975) B2-9.
[8] Surface Active Agent Handbook (Sangyo-tosho, Tokyo, 1960) p. 61 (in Japanese).
[9] J.T. Davies, Turbulence Phenomena (Academic Press, New York and London, 1972) p. 70.